ACS OMEGA

http://pubs.acs.org/journal/acsodf

Article

Optimized Demand-Side Day-Ahead Generation Scheduling Model for a Wind−Photovoltaic−Energy Storage Hydrogen Production System

Kang Chen, Huaiwu Peng,* Junfeng Zhang, Pengfei Chen, Jingxin Ruan, Biao Li, and Yueshe Wang*

Cite This: *ACS Omega* 2022, 7, 43036−43044

Read Online

ACCESS | Metrics & More | Article Recommendations

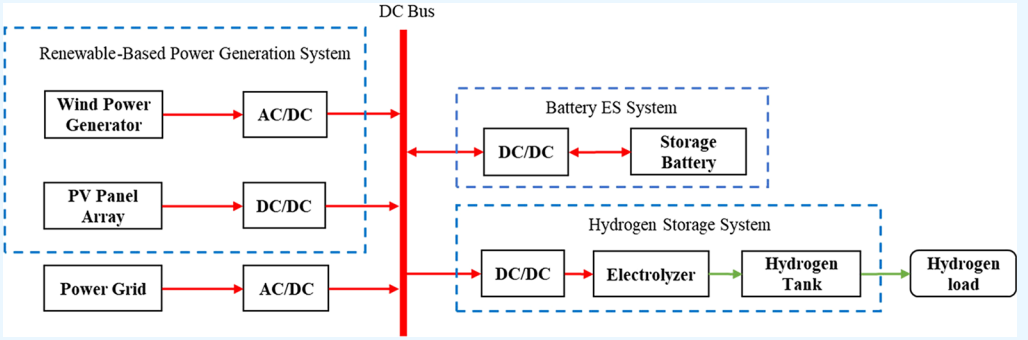

ABSTRACT: This paper proposed an optimized day-ahead generation model involving hydrogen-load demand-side response, with an aim to make the operation of an integrated wind−photovoltaic−energy storage hydrogen production system more cost-efficient. Considering the time-of-use electricity pricing plan, demand for hydrogen load, and the intermittency of renewable energy, the model has the ambition to achieve minimum daily cost of operating a hydrogen production system. The model is power-balanced, fit for energy storage devices, and developed through adaptive simulated annealing particle swarm optimization. Analysis results showed that the proposed optimized scheduling model helped avoid the significant purchase of electric power at peak times and reduced the cost of running the hydrogen production system, ensuring that the daily hydrogen energy produced could meet the daily demand for the gas load. This justified how the model and its algorithm were correctly and efficiently applied.

1. INTRODUCTION

To address resource depletion, global climate change, worsening ecosystems, and other issues arising from the excessive use of fossil fuels, all countries now work to revolutionize their energy sectors and bolster research on the application of renewable energy sources, allowing renewables to play a more critical role. In the case of China, it is on a fast track to carbon-free power. That means that it will reduce the dependence on fossil energy sources and move toward a low-carbon or carbon-free energy mix for peaking emissions and achieving carbon neutrality.

Hydrogen is a secondary renewable source of energy with a high calorific value. There are many different sources of green energy and ways of producing and using it as a fuel. It can also be stored physically as a gas or a liquid, making it safer than conventional fuels. This suggests how important hydrogen is to a shift in energy sources and to carbon neutrality.[1] Free hydrogen does not generally exist in nature, meaning the large-scale use of hydrogen starts with its production. For China, hydrogen is produced from the reforming of fossil fuels and from industrial byproducts, water electrolysis, and new energy (including solar power, biomass, and heat sources).[2] Depending on how carbon is emitted in production, hydrogen can be gray, blue, and green.[3] Hydrogen is labeled green for it mostly produces no carbon, and the variety can only be created through electrochemical water splitting. When the splitting process is powered by renewables (for instance, solar power or wind electricity), hydrogen production can be carbon-free.[4]

The hydrogen production system based on electricity generation from renewables has now been researched worldwide. In a simplistic hydrogen production system designed by Khalilnejad and Riahy[5] the gas was created by directing the electricity from wind turbines and photovoltaic (PV) panels through rectifiers and choppers to electrolyzers, with its amount maximized with the adoption of the imperialist

Received: August 18, 2022
Accepted: October 27, 2022
Published: November 16, 2022

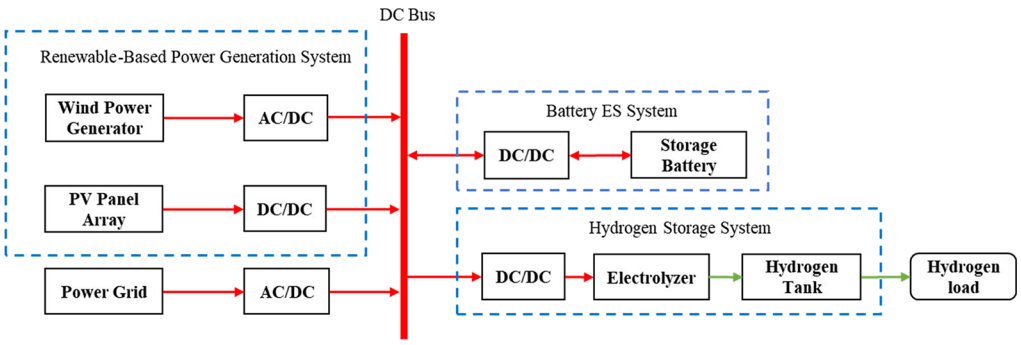

Figure 1. Topology of the wind−PV−ES hydrogen production system.

competitive algorithm. To tackle the fluctuating electricity generation by renewables, Wu et al.[6] put the fluctuation in a certain range by narrowing the gap of power of wind electricity between on-peak and off-peak times with the introduction of storage batteries. By perfecting the hydrogen production system's configuration through iterative optimization, Smaoui et al.[7] proved that the wind−PV approach made energy supply more reliable and power storage more accessible, thus cutting the cost of system installation. Zhang et al.[8] crafted a novel electricity−hydrogen energy system for analyzing the cost-efficiency of the coupled energy storage (ES) system. Through an investigation of the balance between the minimum operating cost and energy storage device of a hybrid electricity−hydrogen system, Pu et al.[9] explored how each system module could perform better. To solve the power balance problem between power generation and demand in energy systems, Latif et al.[10] had developed a prominent dual-level "proportional-integral-one plus double derivative controller". What is more, a recently developed mine blast technique is utilized to optimize the parameters of the newly designed controller. Mojica-Nava et al.[11] proposed a hierarchical microgrid management system based on task sharing and a scheduling strategy based on an evolutionary game theory as a coordination algorithm, which integrates the three main control levels required for microgrid operation and can be regarded as a distributed intelligent system. In another literature, Latif et al.[12] proposed a demand response scheme based on real-time price in a hybrid microgrid system again.

The blend of water electrolysis and power generation by renewable energy sources will be crucial for the large-scale production of green hydrogen. Also, the technology carries significance for the coupling and development of renewables, the dampening of fluctuations in wind−PV electricity generation, and the green, cost-efficient production of hydrogen energy.[13] The topology of the wind−PV−ES hydrogen production system is more complex, and the control variables are numerous and affect each other. Considering the coupling characteristics of multi-energy complementarity, it is necessary to focus on the coordinated control between hydrogen storage and battery energy storage.

In this paper, a day-ahead output optimization scheduling model on the demand-side response of hydrogen load is proposed for the wind−PV−ES hydrogen production system. The model was designed to minimize the day-ahead operating cost of the system. The constraints of each device need to be fully considered. The adaptive simulation annealing particle swarm algorithm is used to solve the operating state of each unit of the system. Finally, case studies proved the model and its algorithm to be effective.

2. WIND−PV−ES HYDROGEN PRODUCTION SYSTEM

2.1. Structure. The wind−PV−ES hydrogen production system can be off-grid and on-grid. The former means hydrogen is created by directing electricity separately from wind and solar power to electrolyzers, while the latter involves water electrolysis with the electricity either from or in excess of the grid that has been connected to wind power generators and PV panels upon inversion.[14]

For now, alkaline water electrolysis (AWE) and water electrolysis based on proton exchange membrane (PEM) are the technologies for commercial hydrogen production systems, with AWE claiming an overwhelming market share. The reason is threefold. First, the power generation of a single hydrogen production system empowered by AWE has now been measured by megawatt and the PEM-based model only by kilowatt. Second, the cost of the AWE-abled system is RMB 3000 per kilowatt, about one-third the price of the PEM-driven system. Third, the system with AWE is expected to work for 10 years, almost twice the time for that with a PEM model.[15]

In this connection, the AWE-based hydrogen production system was employed for our research. As is shown in Figure 1, the wind−PV−ES hydrogen production system comprises wind and PV power sources, an external power grid, storage battery, electrolyzer, hydrogen tank, and other supporting devices. The system was structured by a direct current (DC) bus, with the wind power generator and the PV panel array connected to the bus through converter units to power the electrolyzer. Despite being fluctuant, random, and intermittent, wind energy and solar power inherently complement each other from a spatial−temporal perspective. Also, such reinforcement entails a more efficient power generation system and more stable power delivery.[16]

The time-of-use (TOU) power pricing mechanism means that the system should make full use of wind and PV generation to produce hydrogen while purchasing as little electricity from the grid as possible. Moreover, the built-in hydrogen and battery ES modules would mass-produce the gas in the electrolyzer either at off-peak times or when the wind and PV output are higher, which is when hydrogen goes to the tank, and the battery gains power. Yet, during on-peak hours or when the generation fails to power the electrolyzer, the surplus gas in the tank will supply hydrogen load, and the electricity from storage batteries would ensure that the electrolyzer runs at minimum capacity.

2.2. Operating Properties of the Alkaline Electrolyzer. The operational states of an alkaline electrolyzer are production, standby, and idle. In coupling intermittent renewable energy, the electrolyzer's operational features

https://doi.org/10.1021/acsomega.2c05319
ACS Omega 2022, 7, 43036−43044

worth consideration include the load range, ascent and descent rates, and time for start and shutdown.[17] The alkaline electrolyzer can operate at 15% to 100% of its nominal capacity, making it incompatible with a full range of input power from renewables.[18] Indeed, frequent on-and-off practices not just shorten the life of the electrolyzer but also disrupt how a hydrogen production system powered by wind and solar utilizes energy across the board. With that in mind, the electrolyzer's production state was what the model focused on, and to defuse risks in model optimization, a load limit was introduced as a constraint.

The correlation between the input power and hydrogen production rate of the electrolyzer forms the basis of generation scheduling research. Varela et al.[19] proposed a function (including first- and second-order approximations) to describe the input−output relationship when hydrogen was produced in a commercial alkaline electrolyzer, as shown below:

$$F = 205.31P + 17.85 \tag{1}$$

$$F = -11.24P^2 + 232.7P + 8.89 \tag{2}$$

where P is the input power (MW) of the electrolyzer and F denotes the flow rate (Nm^3/h) of hydrogen production.

Given the need for multiple iterations, a linear approximation is preferred in computing large datasets, particularly for a to-be-optimized model. As such, eq 1 was used to examine the relevance between input and output or between load and flow rate, whereas eq 2 could serve to calculate the flow rate in small-sized models in a more accurate manner. Given that particle swarm optimization (PSO) was adopted to solve the model in this paper, the optimization process requires a number of iterative calculations. Therefore, eq 1 was used to estimate the hydrogen production flow rate of the electrolyzer.

3. OPTIMIZED DAY-AHEAD GENERATION SCHEDULING MODEL FOR THE HYDROGEN PRODUCTION SYSTEM

In this paper, M language and Simulink were employed for simulation modeling. Built in the Simulink environment, the model for wind−PV electricity generation could translate the input meteorological data into the estimated generation of wind and PV power. It focused on the day-ahead scheduling of wind and PV power for hydrogen production, with an aim to minimize the daily cost arising from the process. To this end, adjustments to the charge/discharge power of storage batteries at all-time intervals and the interactive power of electricity bought from the grid were made in line with prediction curves of wind and PV generation and hydrogen load. With adaptive simulated annealing PSO, the optimized day-ahead generation scheduling model for the wind−PV−ES hydrogen production system was created and shown as follows.

3.1. Objective Function. Built on the estimated wind−PV electricity generation using Simulink, hydrogen-load demand, and changing electricity rates, an improved day-ahead generation scheduling model for the wind−PV−ES hydrogen production system was developed. For an operating system, costs arising from putting the electrolyzer, storage battery, and compressor into operation and purchasing power from the grid needed to be factored in. The cost-efficiency of such a system was manifested by the day-ahead operating cost.

$$C_{day} = \sum_{t=t_0}^{t_{end}} C_{ele}P_{ele}^{t}\Delta t + \sum_{t=t_0}^{t_{end}} C_{grid}P_{grid}^{t}\Delta t + \sum_{t=t_0}^{t_{end}} C_{sto}P_{bat}^{t}\Delta t + \sum_{t=t_0}^{t_{end}} C_{com}E_{H_2}^{t}\Delta t$$

In the above equation, C_{day} is the system's day-ahead operating cost (yuan); C_{ele} is the cost (yuan/kW·h) of using the electrolyzer; P_{ele}^{t} represents the electrolyzer's operation power (kW) at time interval t; C_{grid} denotes the rate (yuan/kW·h) at which the system purchase electricity from the grid; P_{grid}^{t}stands for the interactive power (kW) in the case of electricity purchase; C_{sto} indicates the cost (yuan/kW·h) to store per kilowatt-hour in storage batteries; $P_{bat}^{t}$is the actual output (kW) of storage batteries; C_{com} indicates the cost (yuan/N·m^3) of a functioning compressor; $E_{H_2}^{t}$represents the amount (Nm^3) of to-be-compressed hydrogen at time interval t; and Δt is the time interval (1 h).

Among them, the cost of a functioning compressor involves the cost of purchasing and operating the equipment. The price for such equipment changes with its discharge pressure. It takes about RMB 1.8 million to purchase a compressor with a discharge pressure of 20 MPa and capacity of 1000 Nm^3/h, and around RMB 3 million for one with a 45 MPa discharge pressure at the same capacity. The typical lifespan of a compressor is 20 years, with no replacement needed during the period, yet each year, 1% of the initial equipment investment should be used for maintenance.[20] In addition, the electricity consumption of an operating compressor ranges from 0.15 to 0.26 kW·h. Fang et al.[14] reckoned that the energy that a compressor (with a discharge pressure at 20 MPa) consumes to compress one cubic meter of hydrogen averages 0.2 kW·h. Based on the costs of a compressor providing a 20 MPa discharge pressure and its electricity consumption, we assumed that it costs RMB 0.21 to compress one nominal cubic meter (1 Nm^3) of the gas under the proposed model.

3.2. Constraint Conditions. *3.2.1. System Power Balance Constraint.*

$$P_{renew}^{t} + P_{bat}^{t} + P_{grid}^{t} = P_{ele}^{t},\ \forall\ t \in [t_{start}, t_{end}] \tag{4}$$

In the above equation, $P_{renew}^{t}$is the output (kW) of renewable energy sources, or the maximum power of wind−PV electricity generation at time interval t; P_{bat}^{t}signals the charge/discharge power (kW) of the storage battery, with the discharge power value in this paper being positive and the charge power value negative.

3.2.2. Battery ES System Constraint. The storage battery capacity is determined by the capacity stored from the last time slice and by the charge/discharge power and self-discharge amount during that period. The state of charge (SOC) of the battery at time interval t is as follows:

$$S_{bat}^{t} = S_{bat}^{t-1}(1-\sigma) - \eta_c\frac{P_{bat}^{t}\Delta t}{E_{bat}} \tag{5}$$

where S_{bat}^{t}indicates the SOC of the battery at time interval t; σ is the self-discharge rate of the battery; η_c denotes the charge/discharge rate of the battery; and E_{bat} is the total capacity (kW·h) of the battery.

On top of the controlled capacity changes, storage batteries are subject to safety use, which involves the upper and lower limits of the charge/discharge power and capacity and ensures

https://doi.org/10.1021/acsomega.2c05319
ACS Omega 2022, 7, 43036−43044

that the capacity remains the same at the beginning and end of a day.[21]

The upper and lower limits of the charge/discharge power are expressed as follows:

$$\begin{cases} 0 \le P_{bat}^{t} \le P_{dis}^{max} \\ -P_{ch}^{max} \le P_{bat}^{t} \le 0 \end{cases} \quad (6)$$

where P_{ch}^{max} and P_{dis}^{max} represent the power thresholds (kW) of charge and discharge, respectively.

The battery's SOC range is expressed as follows:

$$S_{bat}^{min} \le S_{bat}^{t} \le S_{bat}^{max} \quad (7)$$

where S_{bat}^{min} and S_{bat}^{max} are the lower and upper SOC limits of the storage battery, respectively.

The constraint that makes the capacity equivalent at the beginning and end of a day is expressed as follows:

$$S_{bat}^{t=t_{start}} = S_{bat}^{t=t_{end}} \quad (8)$$

where $S_{bat}^{t=t_{start}}$ and $S_{bat}^{t=t_{end}}$ indicate the battery's SOC at the beginning and end of scheduling, respectively.

3.2.3. Grid-Interactive Power Constraint.

$$P_{grid}^{min} \le P_{grid}^{t} \le P_{grid}^{max}, \forall\, t \in [t_{start}, t_{end}] \quad (9)$$

In the above equation, P_{grid}^{min} and P_{grid}^{max} denote the minimum and maximum power (kW) of the system fueled by purchased electricity.

3.2.4. Electrolyzer Operation Power Constraint.

$$P_{ele}^{min} \le P_{ele}^{t} \le P_{ele}^{max}, \forall\, t \in [t_{start}, t_{end}] \quad (10)$$

In the above equation, P_{ele}^{min} and P_{ele}^{max} are the minimum and maximum operation power (kW) of the alkaline electrolyzer under the production state.

3.2.5. Hydrogen Production Constraint.

$$\begin{cases} M_{H_2}^{t} = M_{H_2}^{t-1} + V_{H_2}^{t} \cdot \Delta t - L_{H_2}^{t} \\ M_{H_2}^{t} \ge 0 \\ M_{H_2}^{t_{end}} = 0 \end{cases} \quad (11)$$

In the above equation, $M_{H_2}^{t}$indicates the amount (Nm^3) of stored hydrogen at time interval t; $V_{H_2}^{t}$is the hydrogen production rate (Nm^3/h) of the alkaline electrolyzer at time interval t; $L_{H_2}^{t}$denotes the demand-side hydrogen load (Nm^3) at time interval t; and $M_{H_2}^{t_{end}}$ is the hydrogen amount stored (Nm^3) at the end of the day-ahead operation scheduling.

To achieve a hydrogen load on the demand side that balances the production and consumption of the gas, the system was not loaded with a large amount of hydrogen after a dispatching cycle was completed. That said, the $M_{H_2}^{t_{end}}$ value in the aforementioned constraint of hydrogen production was 0.

4. OPTIMIZED GENERATION MODEL BASED ON ADAPTIVE SIMULATED ANNEALING PSO

The scheduling of the operating system mentioned above is about strong coupling non-linear optimization and needs to be solved through PSO. In optimization, the particle swarm finds the optimal individual and group values through the fitness function and then has them updated on a continuous basis. There are three critical parameters in iterative computing: inertia weight ω, self-cognition factor c_1, and social cognition factor c_2.

Inertia weight ω can control the development and exploration capabilities of the algorithm. That means that a greater inertia weight comes with a stronger global search capability, making it easier for the particle to identify the optimal solution. When it comes to a smaller weight, the local search capability will increase, and the algorithm is likely to converge.[22] The adaptive inertia weight function is as follows:[23]

$$\omega = (\omega_{max} + \omega_{min})/2 + \tanh(-4 + 8 \times (k_{max} - k)k_{max})\,(\omega_{max} - \omega_{min})/2 \quad (12)$$

where ω_{max} and ω_{min} represent the maximum and minimum values of the inertia weight coefficient, which generally stand at 0.95 and 0.4, respectively; k is the current iteration frequency; and k_{max} denotes the maximum number of iterations.

A particle's search capability is also driven by self-cognition factor c_1 and social cognition factor c_2, with the former directing the particle to fly toward its historical optimal solution while the latter moving the particle toward the optimal position of the swarm. Therefore, the paper introduced learning factors of asynchronous change. That suggested the learning factors changed as iterations continued. In its early iterations, the particle's self-experience weighed heavily on rate computing, while in later iterations, the group or social experience of the particle had a greater weight, which was how the global search capability of the algorithm was enhanced.[24] The equations about the learning factors of asynchronous change are as follows:

$$c_1 = (c_{1min} - c_{1max}) \times \frac{k}{k_{max}} + c_{1max} \quad (13)$$

$$c_2 = (c_{2max} - c_{2min}) \times \frac{k}{k_{max}} + c_{2min} \quad (14)$$

Overall, the equations about the particle swarm's rate and position changes are as follows:

$$\begin{aligned} \nu_i^{(k+1)} &= \lambda[\nu_i^{(k)} + c_1 r_1 (p_{ibest}^{(k)} - x_i^{(k)}) + c_2 r_2 (G_{best}^{(k)} - x_i^{(k)})] \\ x_i^{(k+1)} &= x_i^{(k)} + \nu_i^{(k)} \end{aligned} \quad (15)$$

where $\nu_i^{(k)}$ and $x_i^{(k)}$ are the rate and position of particle i going through iteration k, respectively; r_1 and r_2 are random numbers; p_{ibest} represents the optimal individual position of particle i; and G_{best} is the optimal group position.

Conventional PSO tends to identify the local optimum, while using the simulated annealing (SA) algorithm to search for the optimum, each new solution is taken into consideration, and thus the optimum can be reasonably identified not locally but on a global basis. The better performing p_{ibest} should be more likely to be replaced since it is outperformed by G_{best} under the SA rule. Therefore, it is viable to measure the jump probability of p_{ibest} compared with G_{best}, or

$$e^{-(f_{P_{ibest}} - f_{G_{best}})/T} \quad (16)$$

where f is the fitness value, and if the jump probability serves as the fitness value of p_{ibest}, then the jump probability of p_{ibest} is used to substitute that of G_{best}. The calculation is as follows:[25]

https://doi.org/10.1021/acsomega.2c05319
ACS Omega 2022, 7, 43036−43044

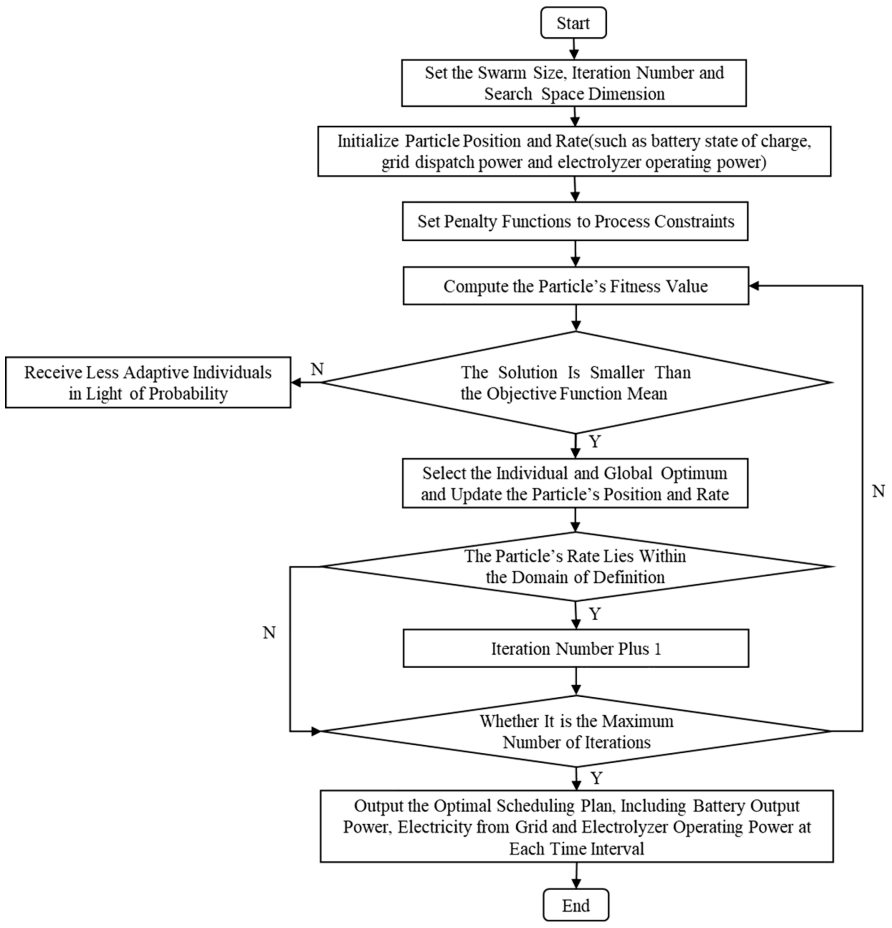

Figure 2. Flow chart of the optimization of day-ahead dispatching.

$$\frac{e^{-(f_{P_{ibest}} - f_{G_{best}})/T}}{\sum_{i=1}^{N} - (f_{P_{ibest}} - f_{G_{best}})/T} \tag{17}$$

Adaptive simulated annealing PSO made an adaptive change to parameters and employed annealing simulation in ways that made the optimizing process faster and more accurate. Given that, the algorithm was adopted to develop the optimized generation scheduling model for the wind−PV−ES hydrogen production system, whose flow diagram is shown in Figure 2.

5. RESULTS AND ANALYSIS

5.1. System Parameters. The researched wind−PV−ES hydrogen production system, consisting of an wind−PV electricity generation subsystem, batteries for energy saving, an alkaline electrolyzer, and other supporting devices, was designed to optimize day-ahead generation scheduling with a 24 h cycle. The upper part was the wind−PV electricity generation model via Simulink, which was tested on a typical day in northwestern China. The meteorological data on the day, such as irradiation intensity, wind speed, and temperature, were input into the model via Simulink for simulation and resulting predictions about wind−PV electricity generation. The curve forecasting wind−PV electricity generation on a typical day is displayed in Figure 3, and two hypothetical hydrogen load scenarios are shown in Figure 4.

The wind−PV−ES hydrogen production system purchases electricity from the grid under the TOU electricity pricing mechanism. The on-peak, regular, and off-peak electricity

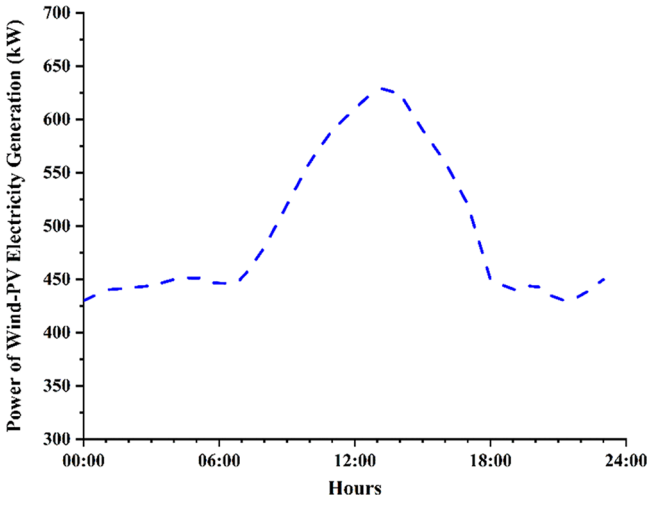

Figure 3. Curve of predictions of wind−PV electricity generation on a typical day.

prices were RMB 0.88, RMB 0.594, and RMB 0.308 per kilowatt-hour, respectively, as shown in Table 1.

The rated power and minimum power of the electrolyzer were, respectively, 800 and 120 kW. The maximum charge/discharge power of the storage battery was 240 kW, and more parameters in the case study are displayed in Table 2.

5.2. Simulation Results and Analysis. *5.2.1. Day-Ahead Generation Scheduling. 5.2.1.1. Hydrogen-Load Demand in*

https://doi.org/10.1021/acsomega.2c05319
ACS Omega 2022, 7, 43036−43044

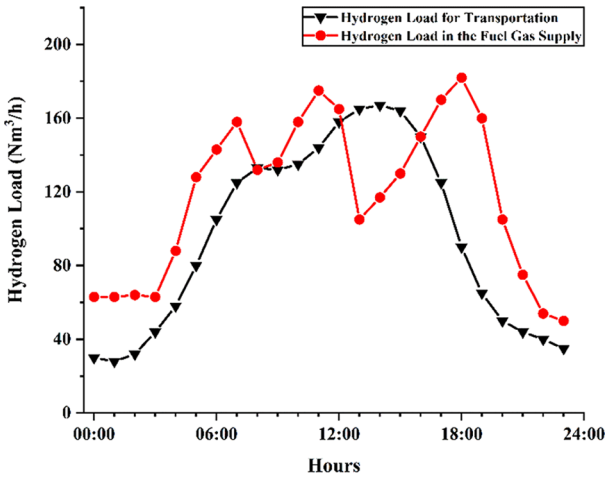

Figure 4. Curves of demand-side hydrogen load on a daily basis.

Table 1. TOU Electricity Pricing Data

time intervals	hours	prices
off-peak	0:00−07:00	0.308
regular	07:00−09:00, 11:00−19:00	0.594
on-peak	09:00−11:00, 19:00−24:00	0.88

Table 2. Case-Study Parameters in Daily Generation Scheduling

Parameters	Values	Parameters	Values
$C_{ele}/\left(元\cdot(\mathrm{kW\cdot h})^{-1}\right)$	0.5	$S_{bat}^{min}/\%$	10
$C_{sto}/\left(元\cdot(\mathrm{kW\cdot h})^{-1}\right)$	0.05	$S_{bat}^{max}/\%$	90
$P_{grid}^{min}/\mathrm{kW}$	0	η_c	1
$P_{grid}^{max}/\mathrm{kW}$	600	$\sigma/\%$	4.6

Transportation. Figure 5 shows the scheduling of each operating unit of the wind−PV−ES hydrogen production system to meet the daily demand for hydrogen load in transportation. Figure 6 displays the SOC of the battery energy storage system. Also, Figure 7 illustrates how fast the system produces hydrogen and how much gas is stored under day-ahead scheduling.

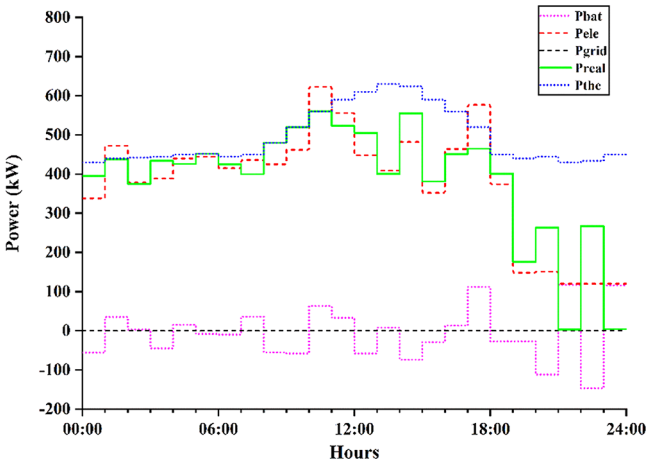

Figure 5. Operational status of each system unit under day-ahead scheduling for meeting hydrogen-load demand in transportation.

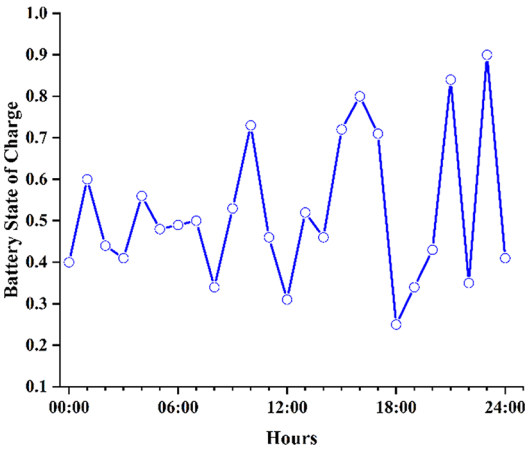

Figure 6. Battery's SOC under day-ahead scheduling on the demand side of hydrogen load in transportation.

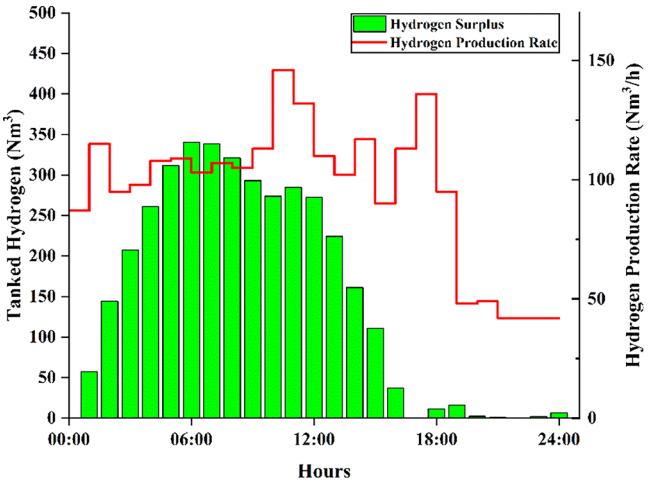

Figure 7. System hydrogen production rate and the amount stored under day-ahead scheduling on the demand side of hydrogen load in transportation.

As shown in Figure 5, the real wind−PV output value P_{real} is always outnumbered by the maximum theoretical output value P_{the}, suggesting that the system remains power-balanced from the beginning to end. In this case, wind−PV electricity generation and energy stored in the battery can power the electrolyzer to produce hydrogen for a one-day supply of fuel gas without needing power from the grid. When wind−PV generation is in surplus, the battery will be charged for storing energy that can fuel the electrolyzer in case of greater demand for hydrogen load and insufficient wind−PV generation.

Figure 6 shows how the storage batter levels out peaks in electricity use. In the case of insufficient wind and solar power, the electrolyzer can still be fueled by the stored battery energy. That ensures that the hydrogen produced by the system meets the demand for hydrogen load in the fuel gas supply. When wind−PV electricity generation can sustain the electrolyzer, the storage battery in the optimized model is not likely to operate, resulting in lower daily operating costs for the system.

As is shown in Figure 7, the optimized model tends to mass-produce and store hydrogen in the case of greater wind−PV

https://doi.org/10.1021/acsomega.2c05319
ACS Omega 2022, 7, 43036−43044

electricity generation. That aims at sustaining the supply of hydrogen as the demand for hydrogen load goes higher over time. But, when such demand dwindles, the electrolyzer creates the gas at a slower rate, ensuring that the amount produced can be consumed on the same day. That makes the hydrogen production system more cost-efficient as it meets the demand for hydrogen load and reduces its daily operating costs.

5.2.1.2. Hydrogen-Load Demand in the Fuel Gas Supply. Figure 8 shows the scheduling of each operating unit of the

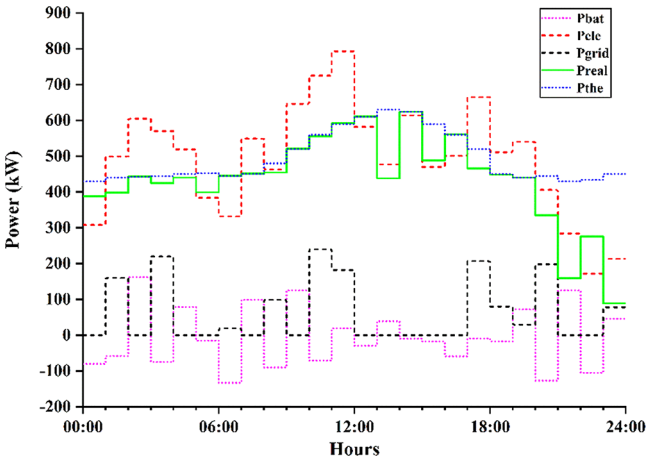

Figure 8. Operational status of each system unit under day-ahead scheduling for meeting the hydrogen-load demand in the fuel gas supply.

wind−PV−ES hydrogen production system to meet the daily demand for hydrogen load in the supply of fuel gas. Figure 9 illustrates the battery's SOC. Figure 10 displays how fast the system produces hydrogen and how much gas is stored.

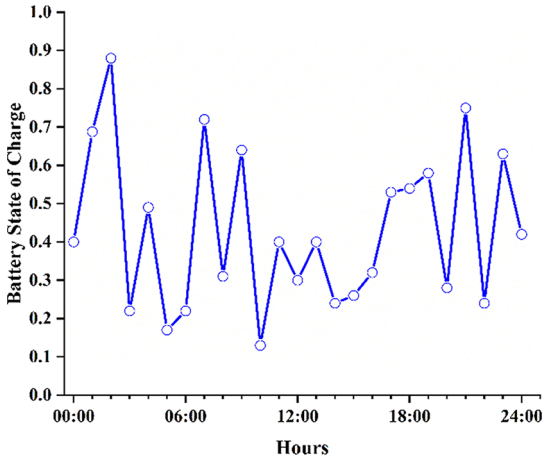

Figure 9. Battery's SOC under day-ahead scheduling on the demand side of hydrogen load in the fuel gas supply.

As is illustrated in Figure 8, to satisfy the demand for hydrogen load in the fuel gas supply, the system is likely to purchase electricity from the grid during regular or off-peak hours (such as 01:00−02:00, 03:00−04:00, 10:00−12:00, and 17:00−19:00) when the electrolyzer mass-produces hydrogen for the sake of storage. Figures 9 and 10 show that the system tends not to buy electricity during on-peak hours, meaning low-priced electricity will complement the insufficient wind and solar power to maintain the needed hydrogen levels. At the

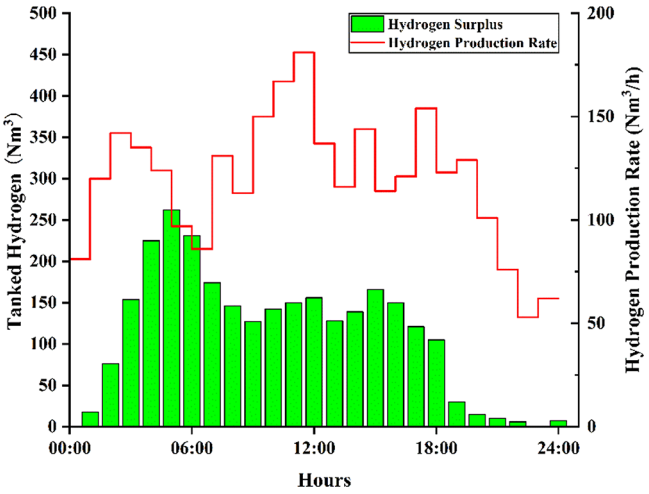

Figure 10. System hydrogen production rate and the amount stored under day-ahead scheduling on the demand side of hydrogen load in the fuel gas supply.

same time, the battery will be charged for storing energy. This way, the system can produce hydrogen through electrolysis and store the gas in tanks in the case of insufficient wind−PV electricity generation or greater demand for hydrogen load.

5.2.2. Impact of Algorithms on Model Results. In solving a model through conventional PSO, iterative computations would probably lead to a local solution, as opposed to a global one. In this paper, we proposed an algorithm by adding a simulated annealing operator and adaptive inertia weight to it, thus making it more capable of searching for the optimal solution on a global basis with adaptive changes to crucial PSO parameters. A blend of conventional and proposed algorithms makes the optimal global solution for the model possible as the swarm is further diversified.

Take the results from the model for hydrogen load in transportation as an example. It was difficult for traditional PSO to either converge or obtain an optimal solution in solving a model, and the daily operating cost of the wind−PV−ES hydrogen production system generally surpassed RMB 6.8 × 10^3. However, the adaptive simulated annealing PSO lowered the cost by 24% to only about 5.2 × 10^3. That justified how the proposed optimization algorithm was feasible to make the system's day-ahead scheduling more cost-efficient.

Figure 11 displays the fitness value curve of the proposed algorithm during a search process. It is found that the algorithm meets expected requirements, as evidenced by its continuous search for an optimal global solution despite the emergence of a feasible one locally.

6. RESULTS AND DISCUSSION

The paper proposed an optimized demand-side day-ahead generation scheduling model for the wind−PV−ES hydrogen production system. The model integrated wind−PV power generation with hydrogen production and storage, as well as battery energy storage. Under the TOU electricity pricing mechanism, we developed the system's day-ahead scheduling for the coordinated operation of each unit. Moreover, hydrogen production satisfies the demand for hydrogen load in a way that better consumes wind and solar power and makes the system's operation more cost-efficient. Compared to conventional PSO, the adaptive simulated annealing PSO proved more feasible in optimizing the economic operation

https://doi.org/10.1021/acsomega.2c05319
ACS Omega 2022, 7, 43036−43044

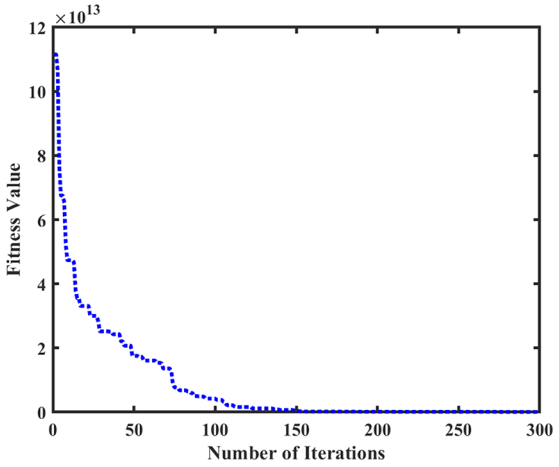

Figure 11. Fitness value of adaptive simulated annealing PSO.

and scheduling of the system and was not likely to settle for an optimal local solution. This met the requirements of the optimized day-ahead scheduling for the wind−PV−ES hydrogen production system. Analysis results from the optimized scheduling of the proposed model in different hydrogen-load scenarios showed that the model and its algorithm were efficient and viable in consuming wind and solar power, reducing costs of system operations, and meeting the demand for hydrogen load.

AUTHOR INFORMATION

Corresponding Authors

Huaiwu Peng − *Institute of Solar Engineering Technology, Northwest Engineering Corporation Limited, PowerChina, Xi'an 710065, China*; Email: phive@163.com

Yueshe Wang − *State Key Laboratory of Multiphase Flow in Power Engineering, Xi'an Jiaotong University, Xi'an 710049, China*; Email: wangys@mail.xjt.u.edu.cn

Authors

Kang Chen − *Institute of Solar Engineering Technology, Northwest Engineering Corporation Limited, PowerChina, Xi'an 710065, China*; orcid.org/0000-0002-9303-5813

Junfeng Zhang − *Institute of Solar Engineering Technology, Northwest Engineering Corporation Limited, PowerChina, Xi'an 710065, China*

Pengfei Chen − *Institute of Solar Engineering Technology, Northwest Engineering Corporation Limited, PowerChina, Xi'an 710065, China*

Jingxin Ruan − *State Key Laboratory of Multiphase Flow in Power Engineering, Xi'an Jiaotong University, Xi'an 710049, China*

Biao Li − *State Key Laboratory of Multiphase Flow in Power Engineering, Xi'an Jiaotong University, Xi'an 710049, China*

Complete contact information is available at: https://pubs.acs.org/10.1021/acsomega.2c05319

Notes

The authors declare no competing financial interest.

ACKNOWLEDGMENTS

This work was supported by the Innovation Capability Support Program of Shaanxi (grant no. 2022KJXX-92) and Key Research and Development Program of Shaanxi (grant no. 2022GY-186).

REFERENCES

(1) Zou, C. N.; Li, J. M.; Zhang, X.; Jin, X.; Xiong, B.; Yu, H.; Liu, X. D.; Wang, S. Y.; Li, Y. H.; Zhang, L.; et al. Industrial status, technological progress, challenges and prospects of hydrogen energy. *Nat. Gas Ind.* **2022**, *42*, 1−20.

(2) Cao, W. J.; Zhang, W. Q.; Li, Y. F.; Zhao, C. H.; Zheng, Y.; Bo, Y. U. Current status of hydrogen production in China. *Prog. Chem.* **2021**, *33*, 2215−2244.

(3) Li, S.; Shi, Y. X.; Cai, N. S. Progress in hydrogen production from fossil fuels and renewable energy sources for the green energy revolution. *J. Tsinghua Univ. (Sci. Technol.)* **2022**, *62*, 655−662.

(4) Zhang, C. R. Development prospect and challenge of green hydrogen in a carbon-neutral era. *Green Pet. Petrochem.* **2022**, *7*, 6−10.

(5) Khalilnejad, A.; Riahy, G. H. A hybrid wind-PV system performance investigation for the purpose of maximum hydrogen production and storage using advanced alkaline electrolyzer. *Energy Convers. Manage.* **2014**, *80*, 398−406.

(6) Wu, X.; Wang, X. L.; Li, J.; Guo, J. L.; Zhang, K.; Chen, J. A joint operation model and solution for hybrid wind energy storage systems. *Proc. CSEE* **2013**, *33*, 10−17.

(7) Smaoui, M.; Abdelkafi, A.; Krichen, L. Optimal sizing of stand-alone PV/wind/hydrogen hybrid system supplying a desalination unit. *Sol. Energy* **2015**, *120*, 263−276.

(8) Zhang, Z. H.; Zhou, J.; Zong, Z.; Chen, Q. C.; Zhang, P.; Wu, K. Development and modeling of a novel electricity-hydrogen energy system based on reversible solid oxide cells and power to gas technology. *Int. J. Hydrogen Energy* **2019**, *44*, 28305.

(9) Pu, Y. C.; Li, Q.; Chen, W. R.; Huang, W. Q.; Hu, B. B.; Han, Y.; Wang, X. Energy management for islanded DC microgrid with hybrid electric-hydrogen energy storage system based on minimum utilization cost and energy storage state balance. *Power Syst. Technol.* **2019**, *43*, 918−927.

(10) Latif, A.; Hussain, S. M. S.; Das, D. C.; Ustun, T. S. Design and Implementation of Maiden Dual-Level Controller for Ameliorating Frequency Control in a Hybrid Microgrid. *Energies* **2021**, *14*, 2418.

(11) Mojica-Nava, E.; Macana, C. A.; Quijano, N. Dynamic Population Games for Optimal Dispatch on Hierarchical Microgrid Control. *IEEE Trans. Syst., Man, Cybern.: Syst.* **2014**, *44*, 306.

(12) Latif, A.; Paul, M.; Das, D. C.; Hussain, S. M. S.; Ustun, T. S. Price Based Demand Response for Optimal Frequency Stabilization in ORC Solar Thermal Based Isolated Hybrid Microgrid under Salp Swarm Technique. *Electronics* **2020**, *9*, 2209.

(13) Jing, T.; Chen, G.; Wang, Z. H.; Xu, P. J.; Li, G. C.; Jia, M. X.; Wang, Y. S.; Shi, J. W.; Li, M. T. Research overview on the integrated system of wind-solar hybrid power generation coupled with hydrogen-based energy storage. *Electr. Power* **2022**, *55*, 75−83.

(14) Fang, S. J.; Shao, Z. F.; Zhang, C. M. Economic analysis on on-grid wind power coupling with hydrogen-production system. *Energy Technol. Econ.* **2012**, *24*, 39−43.

(15) Li, Y. Y.; Deng, X. T.; Gu, J. J.; Zhang, T.; Guo, B.; Yang, F. Y.; OuYang, M. G. Comprehensive review and prospect of the modeling of alkaline water electrolysis system for hydrogen production. *Automot. Eng.* **2022**, *44*, 567−582.

(16) Du, H.; Lv, H.; Yang, D. J. Simulation research progress of wind/photovoltaic (PV) hydrogen system. *Chin. J. Power Sources* **2017**, *41*, 173−175.

(17) Lüke, L.; Zschocke, A. Alkaline water electrolysis: efficient bridge to CO2-emission-free economy. *Chem. Ing. Tech.* **2020**, *92*, 70.

(18) Brauns, J.; Turek, T. Alkaline water electrolysis powered by renewable energy: a review. *Processes* **2020**, *8*, 248.

(19) Varela, C.; Mostafa, M.; Zondervan, E. Modeling alkaline water electrolysis for power-to-x applications: a scheduling approach. *Int. J. Hydrogen Energy* **2021**, 9303.

(20) Shao, Z. F.; Wu, J. L. Capacity configuration optimization of hydrogen production from wind and photovoltaic power based on dynamic electricity price. *Acta Energ. Sol. Sin.* **2020**, *41*, 227−235.

https://doi.org/10.1021/acsomega.2c05319
ACS Omega 2022, 7, 43036−43044

(21) Yuan, T. J.; Wan, Z.; Wang, J. J.; Zhang, D.; Jiang, D. F. The day-ahead output plan of hydrogen production system considering the start-stop characteristics of electrolytic cell. *Electr. Power* **2022**, *55*, 101−109.
(22) Xu, H. Y. Research on inertia weight in particle swarm optimization and case analysis. *Software Guide* **2013**, *12*, 57−60.
(23) Yan, Q. M.; Ma, R. Q.; Ma, Y. X.; Wang, J. J. Adaptive simulated annealing particle swarm optimization algorithm. *J. Xidian Univ.* **2021**, *48*, 120−127.
(24) Hao, H.; Zhang, T. Y. Research on optimizing unit load distribution based on improved particle swarm optimization. *Sci. Technol. Innovation Herald* **2019**, *16*, 106−108.
(25) Zhang, DF. *MATLAB R2020a Intelligent Algorithm and Case Study*; Publishing House of Electronics Industry: Beijing, 2021.

https://doi.org/10.1021/acsomega.2c05319
ACS Omega 2022, 7, 43036−43044